[S. Richter, T. Kathrotia, C. Naumann, T. Kick, N. Slavinskaya, M. Braun-Unkhoff, U. Riedel, Experimental and modelling study of Farnesane, Fuel 215 (2018) 22-29.]

The original publication is available at www.elsevier.com

https://doi.org/10.1016/j.fuel.2017.10.117

EXPERIMENTAL AND MODELING STUDY OF FARNESANE

Sandra Richter*, Trupti Kathrotia, Clemens Naumann, Thomas Kick, Nadezhda Slavinskaya, Marina Braun-Unkhoff, Uwe Riedel

Institute of Combustion Technology, German Aerospace Center (DLR), Pfaffenwaldring 38-40, 70569 Stuttgart, Germany

*Corresponding author: Sandra.Richter@dlr.de

Abstract

Several alternative synthetic fuels are in discussion as a replacement for conventional fuels like Jet A-1 to cope with limited supplies of crude oil as well as their emissions connected with its use such as the greenhouse gas CO_2. One of the alternative fuels which have received high attention recently is farnesane (2,6,10-trimethyldodecane), a biofuel produced from sugar using a biotechnological process. In this paper, combustion characteristics of farnesane were investigated by measuring its ignition delay time using a shock tube at elevated pressure (16 bar) and two different stoichiometries (φ = 1.0 and φ = 2.0) and the laminar burning velocity at atmospheric and elevated pressures (1, 3, and 6 bar). These results were compared to a conventional Jet A-1 fuel showing that farnesane has a similar combustion behavior. Furthermore, a reaction model was developed capable to predict the measured combustion properties. The calculation of the ignition delay times yields excellent results when compared to the measurements; the computations of the laminar flame speeds are in good agreement with the measurements. In addition, the reaction model was analyzed to get further insight into the main reaction steps of farnesane oxidation.

Keywords: Farnesane, biofuel, ignition delay time, laminar flame speed, shock tube, reaction modeling

1. INTRODUCTION

Until now crude oil is the dominant source of fuels for transportation. But the use of conventional transportation fuels is connected with at least two problems: They are produced from crude oil, which is an exhaustible raw material, and their combustion is connected with emissions such as the greenhouse gases CO_2 and water vapor (H_2O). Further emissions are nitrogen oxides (NO_x), and particulate matter [1 – 3].

Over the past years different liquid synthetic fuels were developed either based on other fossil resources, like Gas-to-Liquid fuels (GtL) made from natural gas, Coal-to-Liquid fuels (CtL) from coal [4 – 6], or obtained from biomass (BtL). Typical organic raw materials are sugar, vegetable oils, and fatty acids but also wood-based biomass [1, 2, 7, 8]. At present, alternative aviation fuels are predominantly developed as drop-in-fuels because of the long lifetimes of jet engines and due to stricter regulations [1]. In general, conventional jet fuel has to comply with the standard ASTM D1655 and synthetic jet fuel with ASTM D7566 [2, 8] ensuring that the combustion is reliable and safe under all flight conditions, *e.g.* cold temperatures at high altitude. Moreover, this certification assures that the new synthetic jet fuel is compatible with current engines and technology and that synthetic jet fuel blends are interchangeable with conventional aviation fuels to prevent any logistics or storage problems at airports that may arise due to the handling of different fuels.

The use of coal or natural gas as feedstock for synthetic fuel production via the Fischer-Tropsch process (CtL or GtL) led to the first approved alternative fuels for blending up to 50 %. Moreover a CtL production process exists which yields a fully synthetic jet fuel (FSJF), meaning that it can be used as a replacement of crude oil based fuels without blending [2]. This is of course an alternative to the use of crude oil, but it is neither sustainable nor can a reduction of CO_2-emissions be expected. However, Fischer-Tropsch technology also allows the use of biomass as raw material to produce synthetic fuels; but to our knowledge up to now no commercial or large scale plant is operational using this technology.

To benefit from biofuels – a sustainable replacement for crude oil based fuels, reduction of overall emissions, including the greenhouse gas CO_2 [3, 9] – other fuels, processes and technologies were developed. Approved in 2014 [10], a biofuel for aviation which can be used as a drop-in-fuel is farnesane [8], a branched alkane with 15 carbon atoms as it is shown in Fig. 1. Its chemical name is 2,6,10-trimethyldodecane; for a better readability, only the name farnesane is used in this paper. The production of farnesane has three major steps. At first, sugar is fermented by yeast to farnesene, a molecule with four double bonds [11]. The second step is the hydrogenation from farnesene to farnesane which in the last step is purified by distillation [8]. Whereas Jet A-1 is a multicomponent mixture [2] farnesane is a single component with a molecular size being in the upper range of the molecular size distribution typically found in Jet A-1. Since it is a pure component only some physical properties (selected properties are shown in Tab. 1) are in the acceptable range for aviation fuels like boiling point or flashpoint. Density and viscosity are out of the range [8], so consequently farnesane is approved as a blending component to Jet A-1 up to an amount of 10 % only. For comparison, HEFA (hydrotreated esters and fatty acids) kerosene, a biofuel made from vegetable oils consisting of different, predominantly branched alkanes, is approved as a drop-in-fuel up to 50 % [8]. Passenger flights from Florida to Sao Paulo [12, 13] and in Germany [13, 14] were already operated using a 10 % farnesane blend as jet fuel as well as a delivery flight of an Airbus A350 from Toulouse to Hong Kong [15].

Since farnesane is not only considered as a biofuel for aviation but also as an alternative for diesel fuel [16], few studies have focused on the ignition and decomposition behavior [16 – 19]. Moreover, engine emissions tests were performed with jet fuel [3, 8] as well as diesel blends [20]. Recently speciation data for farnesane were published [21] providing information on its reaction behavior and product distribution.

The aim of the current paper is to present new experimental data for two major combustion properties, ignition delay time and laminar burning velocity, as well as a first reaction model devel-

oped to describe the combustion of farnesane; the model's performance with respect to the experimentally measured combustion properties will be discussed.

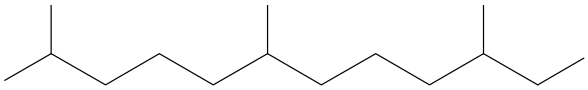

Fig. 1: Chemical structure of the farnesane molecule (2,6,10-trimethyldodecane), $C_{15}H_{32}$

2. Experimental Study

Two global combustion properties of farnesane were investigated: the ignition delay time and the laminar burning velocity. The obtained results were compared to measurements of a conventional Jet A-1 fuel. An overview about selected physical properties of farnesane as well as of the specific Jet A-1 used in the experiments is given in Tab. 1.

Tab. 1: Selected physical properties of farnesane and the specific Jet A-1 used in this study (data of farnesane are taken from [8], formula of Jet A-1 are empirically determined from its H/C ratio of 1.9)

	Farnesane	**Jet A-1** [22]
Formula	$C_{15}H_{32}$	$C_{12}H_{23}$
Molar mass (g/mol)	212.41	167
Density at 288 K (g/cm³)	0.7731	0.8035
Boiling temperature (K)	520	423 – 551
Flashpoint (K)	380.65	313.15
Viscosity at 253 K (mm²/s)	14.13	4.122

2.1. Ignition delay time

Experimental Setup

The experiments were carried out in a high pressure shock tube with an internal diameter of 46 mm. It was divided by aluminium diaphragms into a driver section of about 10 m and a driven section of 3.25 m in length. The driver section was heated to 393 K and loaded with mixtures of helium and argon controlled by Bronkhorst mass flow controllers to achieve tailored interface conditions [23]. The driven section was heated to 453 K and pumped down to pressures below 10^{-4} mbar by a turbomolecular pump. Gas mixtures were prepared in a 5 liter stainless steel storage vessel, which was heated to 180 °C, nitrogen flushed and evacuated using a separate rotary vane pump to obtain pressures below 10^{-2} mbar. For each experiment a new mixture was prepared by injecting the liquid fuel with a syringe onto fibers permanently purged by hot nitrogen which evaporated and transported the fuel into the evacuated vessel. Preheated synthetic air (80 vol-% N_2, 20 vol-% O_2) and nitrogen were added thereafter adjusting equivalence ratio and dilution. All gases were delivered by Linde at purities of N_2: 99.999 %, syn. air: 99.9995 %. After a mixing time of 10 min the fuel-air-N_2 mixture was filled into the shock tube. The optimal mixing period, gas preheat temperatures, and the mixtures' composition were determined and controlled by gas chromatographic analysis monitoring fuel degradation and recovery rate.

The incident shock speed was measured over three 30 mm intervals using four piezo-electric pressure gauges. The temperature and pressure behind the reflected shock wave were computed from the measured incident shock speed and the attenuation using a one-dimensional shock model. For farnesane the thermodynamic data by [24] were used and for Jet A-1 the data of Jet A (g) given by Goos *et al.* [25]. The concentration of Jet A-1 (g) was calculated using its average composition ($C_{12}H_{23}$) and the equivalence ratio of the experiment. The estimated uncertainty in the reflected shock temperature is less than ±15 K throughout the temperature range of our measurements.

The ignition was observed by measuring pressure profiles with piezo-electric gauges (PCB® 112A22 and Kistler® 603B coated with a thin layer of RTV106 high temperature silicone rubber) located at a distance of 1 cm from the end flange. In addition, the CH*-emission at 431 nm, at the same position and through the end flange as well, was selected by a narrow band pass filters (Hugo Anders, FWHM = 5 nm) and measured with a HAMATSU® R3896 photomultiplier in combination with a FEMTO® HLVA-100 logarithmic amplifier. Moreover, two measurement ports at a distance of 7 cm and 10 cm from the end plate were detecting the CH*-chemiluminescence emitted by the propagating deflagration wave. All ignition delay time values shown in this paper were determined by measuring the time difference between the initiation of the system by the reflected shock wave at the end flange and the occurrence of the maximum of the CH*-signal at the side on measurement port 1 cm away from the end plate; this characteristic can be reproduced easily from the corresponding simulations. The experimental setup allows measurements of ignition delay times up to 10 ms depending on the temperature. Post-shock compression effects mainly due to the interaction of incident gas with the attenuated reflected shock wave introduce a time dependent pressure increase $p = p(t)$ with a maximum compression of p_5/p_5 (t=0) = 1.22 at about 8 ms resulting in a temperature increase $T = T(t)$ and thus, in an acceleration of the reactive system towards ignition.

Experimental ignition delay time determination

The ignition delay times of farnesane and Jet A-1 were determined at stoichiometric (φ = 1.0) and fuel-rich (φ = 2.0) conditions. The fuel-synthetic air mixtures were diluted with nitrogen (50 % mixture / 50 % N_2, defined as dilution 1:2). The temperature range was 800 K ≤ T ≤ 1400 K at initial pressures of about 16 bar. A pressure profile as well as radial and axial CH*-emission profiles of a single experiment are presented in Fig. 2: The pressure signal of the farnesane-O_2-N_2 mixture (φ = 1.0, dilution 1:2) at an initial temperature T_i = 883 K and an initial pressure p_i = 16.85 bar (green curve) shows at the very first stage a two-step increase due to the incident and reflected shock wave; this is followed by: (i) a slow pressure increase due to gas dynamic effects as described above without any

145 influence of the fuel's combustion; (ii) a turning point at 2500 µs due to the reflected shock wave
146 passing the contact surface; and (iii) a further increase due to the superposition of gas dynamic ef-
147 fects, caused by the propagation of the reflected shock wave into the driver gas, and the heat release
148 by the ignition. Pressure profiles from experiments without ignition or from non-reactive mixtures of
149 similar acoustic impedance were used to deduce a characteristic pressure profile $p = p(t)$ without
150 distortion due to heat release for modeling ignition delay times.
151

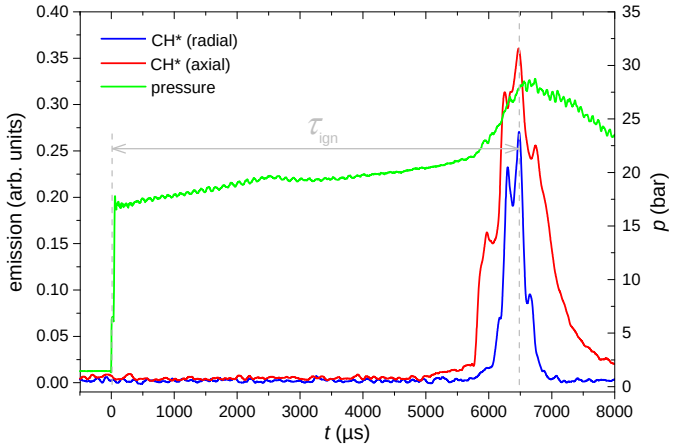

152

153 **Fig. 2: Pressure and emission profiles of a synthetic air-farnesane-N_2 mixture at φ = 1.0, dilution 1:2, T_i = 883 K and**
154 **p_i = 16.85 bar**
155

156 The axial CH*-emission profile (Fig. 2, red line) remains at zero level up to 5000 µs, followed by a
157 steep rise at 5800 µs indicating the start of the ignition process. Please note that the emission signals
158 were amplified by a logarithmic amplifier. The first phase of the ignition process was observed to
159 happen statically, *i.e.* no propagation is detectable. When propagation of the ignition kernel is start-
160 ing, a more or less intense dip or a shoulder in the axial emission profile was observed – here at
161 about 6000 µs – followed by a further increase of the axial emission signal, and from now on also of
162 the radial, due to the formation of the deflagration wave. The time of the maximum CH*-emission at
163 the side port is taken as ignition delay time (Fig. 2, dashed grey line).

164 From the pressure and emission signals of the stoichiometric farnesane mixtures, we have no in-
165 dication to deduce on a two-step ignition process as it has been observed during the ignition process

166 of n-alkanes [26]. Nevertheless, for mixtures at φ = 2.0 and temperatures below 850 K, emission pro-
167 files at 431 nm turn out to show a low level emission within millisecond range accompanied by a
168 slight pressure increase that ceases again until main ignition occurs later.

169 In Fig. 3, the ignition delay times evaluated from the CH*-emission signals are plotted as a func-
170 tion of the reciprocal temperature: Farnesane and for comparison Jet A-1 obtained under the same
171 experimental conditions as described above. The comparison between the different equivalence
172 ratios shows that at temperatures less than 1000 K the ignition delay times of Jet A-1 at φ = 2.0 (Fig.
173 3, blue open triangles) tend to become shorter than at φ = 1.0 (Fig. 3, red open circles), whereas
174 those of farnesane (Fig. 3, solid symbols) do not differ significantly. However, a NTC-effect (Negative
175 Temperature Coefficient), even though less pronounced, cannot be deduced from the farnesane
176 ignition delay time measurements due to their scatter (Fig. 3, blue solid triangles).

177 Above 1000 K, ignition delay times of farnesane and Jet A-1 at both considered φ-values are very
178 similar, although for stoichiometric conditions Jet A-1 (Fig. 3, red open circles) seems to have a slight-
179 ly higher apparent activation energy. This is especially remarkable for temperatures below 1000 K,
180 where ignition delay times of farnesane at φ = 1.0 (Fig. 3, red solid circles) are significantly shorter
181 than those of Jet A-1 (Fig. 3, red open circles). Similar results were obtained from Valco *et al.* [19],
182 who measured ignition delay times of conventional and alternative fuels for temperatures between
183 625 and 735 K using a rapid compression machine. Their work shows that farnesane has shorter igni-
184 tion delay times in the considered temperature range than the jet fuels chosen for comparison.
185

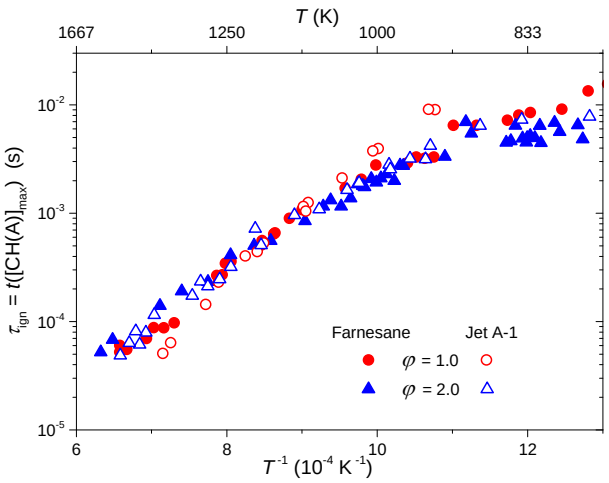

Fig. 3: Ignition delay times (τ_{ign}) of farnesane and Jet A-1, measured with synthetic air and dilution in N_2 (d = 1:2) at equivalence ratio φ and an initial pressure of p_i = 16 bar attributed to the initial reciprocal temperature T_i.

2.2. Laminar burning velocity

Experimental Setup

The laminar burning velocity (S_u) was deduced from the measurement of the cone angle (α) of the flames investigated (see Fig. 4 and equation (1); and also [4, 27, 28]). The flow speed of the unburned gas mixture (v_u) was calculated from the volumetric flow rate measured in the experiment and the cross-section of the nozzle outlet.

$$S_u = v_u \cdot \sin \alpha \quad \textbf{(1)}$$

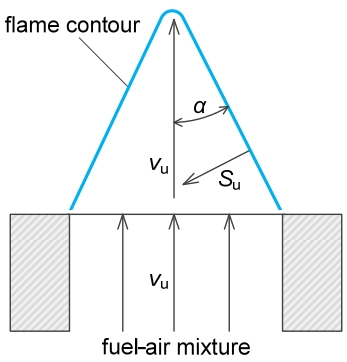

Fig. 4: Determination of the laminar burning velocity S_u (v_u - flow speed of the unburned gas mixture, α - cone angle)

The measurements were performed at a preheat-temperature of 473 K, at pressures of 1, 3 and 6 bar and at an equivalence ratio φ ranging from 0.6 to 2.0 at 1 bar (the range is slightly smaller at elevated pressures). A schematic of the experimental setup is shown in Fig. 5. In the first part of the test rig, which contains the preparation of the fuel-O_2-N_2 mixture, the fuel was vaporized [29] at temperatures from 560 K to 660 K; the exact temperature depends on the fuel (farnesane or Jet A-1) and the pressure in the system. The fuel volume flow was regulated by a HPLC-pump (type LC-20AD, Shimadzu). In order to avoid early oxidation or cracking reactions, the fuel was purged with helium before vaporization; then, mixed at first with nitrogen (Linde, purity 99.999 %) only. During the homogenization with nitrogen, the temperature of the gas-mixture was reduced to the set preheat-temperature of 473 K before the oxygen (Linde, purity 99.95 %) was added. The ratio between nitrogen and oxygen was 79:21 (N_2:O_2); their flow rates were controlled by mass flow controllers (type F-111B, Bronkhorst) calibrated with Cal-Trak (type SL-800-24, Sierra Instruments).

The next part of the setup consists of the burner itself where at the nozzle outlet the gas mixture was burned. To generate elevated pressures, housing of the burner was necessary. To stabilize the flames over a fuel-air-ratio as broad as possible, a coflow was introduced: air at rich conditions ($\varphi \geq 1.0$) and a mixture of 5 % CH_4, 5 % H_2 and 90 % N_2 at lean conditions ($\varphi \leq 1.0$). Due to the use of these different coflows post-combustion processes enable the flame stabilization at rich as well as at lean conditions: During the combustion of a fuel-rich mixture, some hydrocarbons in the hot exhaust gas will get in contact with the oxygen from the surrounding air. Consequently, a post-combustion process takes place. At lean conditions that isn't possible since all hydrocarbons are consumed by the reaction with oxygen; instead excess oxygen remains in the exhaust gas. However, using the CH_4/H_2/N_2-mixture as coflow, the same effect, post combustion, occurs compared to the fuel-rich flame with an air-coflow – a post-combustion in the exhaust gas by the reaction of the remaining oxygen with the reactive components (CH_4 and H_2) of this coflow.

The last part of the setup contains the analysis section. Pictures of the flames were recorded with a CCD-camera (type Imager Intense, LaVision); examples are shown in Fig. 6. The laminar burning velocity was derived from these images by measuring the cone angle and using equation (1) for the flow rate set. The uncertainties, resulting from the accuracies of the mass flow controllers, the cone angle detection and the treatment of the fuel as ideal gas, were estimated to be in the range from 3 % to 12 % depending on the pressure and the fuel-air-ratio; they rose with increasing pressure and φ-difference to stoichiometric conditions.

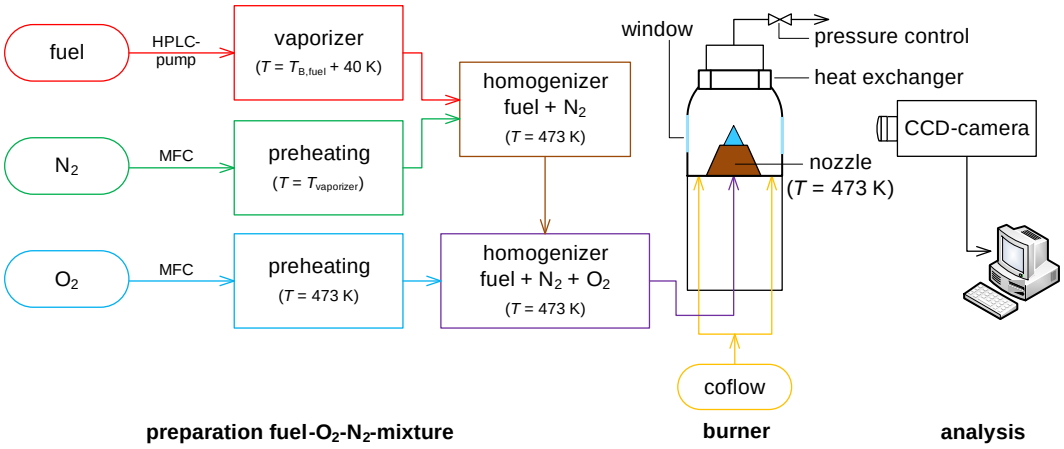

Fig. 5: Experimental setup for measuring the laminar burning velocity via the cone-angle method (MFC - mass flow controller, T_B - boiling temperature)

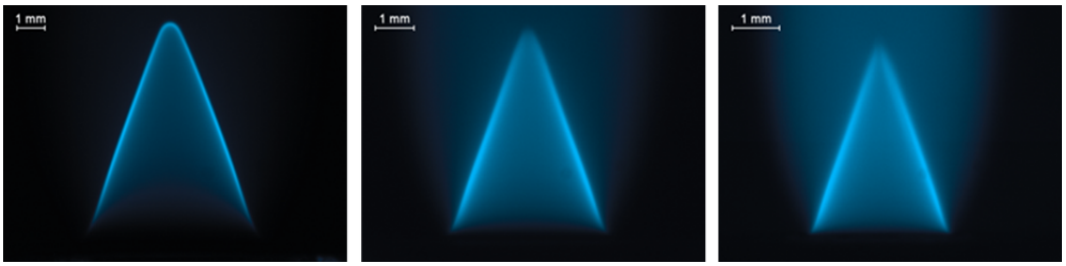

Fig. 6: Typical flame contours of laminar premixed farnesane-air flames at φ = 1.15, T = 473 K, and p = 1 bar (left), p = 3 bar (middle), p = 6 bar (right)

Experimental determination of burning velocity

The results of the measured laminar burning velocities are presented in Fig. 7. It is clearly visible that the laminar burning velocity decreases with increasing pressure and that all curves have a slightly bell-shaped progression. The maxima are obtained at an equivalence ratio between 1.05 and 1.10, as typical for a hydrocarbon flame, with values of 78 cm/s at a pressure of 1 bar, 64 cm/s at 3 bar, and 56 cm/s at 6 bar. For clarity, some error bars, representing the maximum error are plotted in Fig. 7; the larger error bars for p = 6 bar are due to higher fluctuations during the measurement.

For comparison of the laminar burning velocity of farnesane with a conventional jet fuel, measurements of Jet A-1 were performed using the same method. The result of the comparison is also shown in Fig. 7: Farnesane has nearly the same laminar burning velocity compared to Jet A-1 at all three pressures, with insignificant deviations at the higher pressures. This similarity between crude oil based jet fuels and alternative fuels was also found in previous studies, *e.g.* [2, 4 – 6, 30, 31] and is confirmed for farnesane by this work.

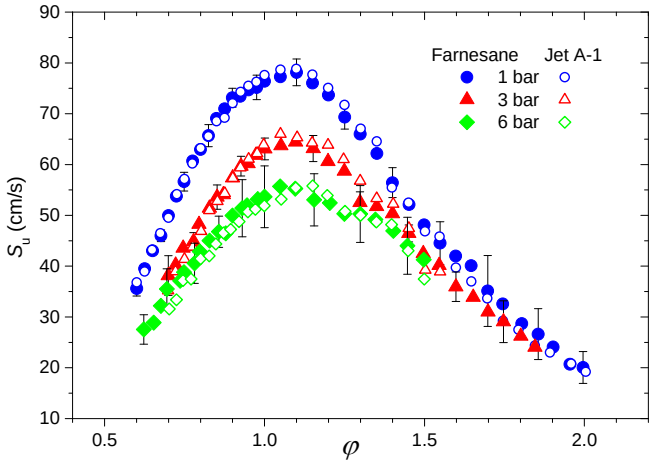

Fig. 7: Laminar burning velocity (S_u) of farnesane- and Jet A-1-air mixtures at a preheat-temperature of 473 K (φ - equivalence ratio)

3. Modeling Study

Reaction mechanism of farnesane oxidation

Farnesane is a branched hydrocarbon (iso-alkane) with three methyl groups attached to the main C_{12}-linear hydrocarbon molecule at C-position 2, 6, and 10 (see Fig. 1). This branching pattern makes it a complex molecule for reaction modeling. The reaction sub-model of farnesane is implemented in our in-house existing reaction model that can describe the oxidation of normal- and iso-alkanes up to C_{12} [32, 33]; with the new sub-model of farnesane it contains now 227 species and 1443 reactions. The full mechanism is available from the authors upon request.

The reaction sub-model of farnesane considers the depletion of farnesane by thermal decomposition as well as by H-atom abstraction reactions via various radicals present in the system, mainly H, O, OH, and CH_3. For simplicity, the reaction model is lumped to primary, secondary, and tertiary carbon and radical sites, as shown in Fig. 8.

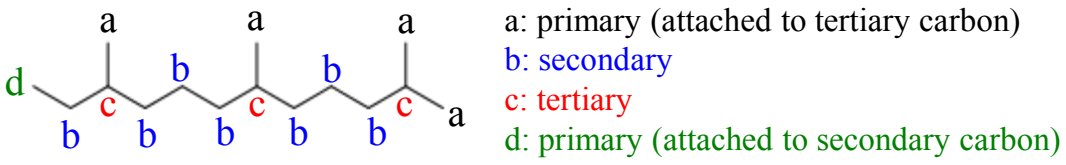

Fig. 8: Nomenclature used for lumping isomers to primary, secondary, and tertiary radical sites

Thus, for the farnesane molecule there are 5 primary, 7 secondary and 3 tertiary carbons which are lumped in order to model the H-abstraction reactions. In addition, the reaction model also includes decomposition of alkyl radicals such as $iC_{15}H_{31}$ formed by H-abstraction of the fuel molecule, or formed from the unimolecular decomposition of farnesane such as $iC_{12}H_{25}$ and $iC_{13}H_{27}$ to olefins (a species dictionary is provided as supplemental material to clarify structure of isomers). In addition, radical isomerization reactions as well as reactions describing olefin decomposition are also an important part of the high temperature farnesane chemistry. The olefins are mainly formed by the β-scission of the first fuel radical $iC_{15}H_{31}$ and they ($iC_{15}H_{30}$, $iC_{14}H_{28}$) are added to the model. Additionally, reactions addressing the low temperature farnesane chemistry are added to the mechanism. The rate coefficients for the above mentioned reactions are estimated from analogies to similar molecules available in the base mechanism or taken from literature as described below.

The thermal decomposition of farnesane ($iC_{15}H_{32}$) forms either ($iC_{15}H_{31}$) and H-atoms or leads to smaller alkyl radicals considering the decomposition at each carbon atom of the parent molecule. The rate coefficients of these reactions have been considered from the analogy of $iC_{11}H_{24}$ species as included in the base mechanism [32]. The thermal decomposition produces thirteen alkyl radicals:

$iC_{15}H_{32} \leftrightarrow b\text{-}iC_{13}H_{27} + C_2H_5$ (R1)

$\leftrightarrow d\text{-}iC_{12}H_{25} + iC_3H_7$ (R2)

$\leftrightarrow d\text{-}iC_{11}H_{23} + sC_4H_9$ (R3)

$\leftrightarrow d\text{-}iC_{11}H_{23} + iC_4H_9$ (R4)

$\leftrightarrow iC_8H_{17} + iC_7H_{15}$ (R5)

$\leftrightarrow iC_9H_{19} + iC_6H_{13}$ (R6)

$\leftrightarrow a\text{-}iC_{10}H_{21} + iC_5H_{11}$ (R7)

The H-abstraction reactions of farnesane are:

$iC_{15}H_{32} + R \leftrightarrow a/b/c/d\text{-}iC_{15}H_{31} + RH$ where R = H/O/OH/CH_3 (R8)

The H-atom abstraction reactions as well as the thermal decomposition reactions are lumped to one secondary (b-site), one tertiary (t-site) and two primary radicals namely a-site (C-atom attached to adjoining tertiary carbon) and d-site (C-atom attached to adjoining secondary carbon) based on the nomenclature used in Slavinskaya *et al.* [32]. The rate coefficients of these reactions are based on analogous reactions described by Curran *et al.* [34] as part of their iso-octane reaction model.

Each of the alkyl radicals formed undergoes β-scission and decomposes to form olefins (such as $iC_{15}H_{30}$, $iC_{14}H_{28}$, $iC_{11}H_{22}$, $iC_{10}H_{20}$, iC_9H_{18}, iC_8H_{16}, iC_7H_{14}, iC_6H_{12}, iC_5H_{10}, and iC_4H_8) and alkyl radicals such as $iC_{13}H_{27}$, $iC_{12}H_{25}$, $iC_{11}H_{23}$, $iC_{10}H_{21}$, iC_9H_{19}, iC_8H_{17}, iC_7H_{15}, iC_6H_{13}, iC_5H_{11}, iC_4H_9, iC_3H_7, C_2H_5, and CH_3. Most of the products of the decomposition of the radicals are branched olefins and iso-alkyl radicals. The reactions are available in the supplementary material. The rate coefficients of these reactions are

from the recommendations given by Ratkiewicz and Truong [35]; their rate predictions were obtained by applying transition state theory, with derived reaction rates of C−C bond scission in a wide range of alkyl radicals. In addition, they provided a general rate equation which − depending on the H-abstraction sites − can be used to obtain a rate for any reaction belonging to this class depending on the abstracting radical site *i.e.* primary, secondary and tertiary radicals.

The $iC_{15}H_{31}$ radicals formed are isomerized to 4 different isomers:

a-$iC_{15}H_{31}$ ↔ b-$iC_{15}H_{31}$ ↔ c-$iC_{15}H_{31}$↔ d-$iC_{15}H_{31}$

The reaction rates of $iC_{15}H_{31}$ isomerization are based on the reaction rate expressions determined experimentally and numerically by Awan *et al.* [36] for the analogous 5-methylhex-1-yl radical. They studied isomerization and decomposition reaction rate in the temperature and pressure range of 500 to 1900 K and 0.1 to 1000 bar.

The farnesane reaction sub-model also includes new decomposition reactions of olefins ($iC_{14}H_{28}$, $iC_{15}H_{30}$), produced during fuel decomposition, which were not present in the base mechanism [32, 33].

In addition, the reaction model includes preliminary low temperature farnesane chemistry: alkyl peroxide radical formation; isomerization to hydroperoxyl alkyl radical; formation and decomposition of the hydroperoxyl alkyl peroxy radical as well as the keto hydroperoxide decomposition. The reaction rates of the low temperature farnesane chemistry are adapted by the analogy to the $iC_{11}H_{24}$ reactions which is already part of the base mechanism. The farnesane sub-model contains 17 species and 84 forward reactions. The entire farnesane sub-model is provided in the supplementary material.

Calculation of global combustion properties

The reaction mechanism developed for describing the farnesane oxidation is used for calculating both global fuel characteristics, ignition delay time and burning velocity, measured experimentally.

The predictions of ignition delay times and laminar flame speeds are based on the zero-dimensional (0-D) homogeneous closed reactor model and the one-dimensional laminar freely propagating flame model respectively, as implemented in the software-package Chemical WorkBench (CWB) [37] used for the calculation.

Ignition delay times are calculated with the initial mixture composition, the initial temperature behind the reflected shock wave and the measured pressure profile as input. The ignition delay times are determined from the maximum of CH*-profiles. Laminar flame speeds are calculated with fuel-oxidizer mixture composition, preheat-temperature, and pressure as required input. The flames are calculated considering thermal diffusion using a multi-component transport model. The thermo-chemical data for the farnesane sub-model specific species (Farnesane, $iC_{15}H_{31}$, $iC_{15}H_{30}$, $iC_{14}H_{28}$, $iC_{13}H_{27}$, $iC_{12}H_{25}$, $C_{15}H_{31}O_2$, $C_{15}H_{30}OOH$, $O_2C_{15}H_{30}OOH$, $OC_{15}H_{29}OOH$) are obtained from the RMG [24] which are based on group additivity.

4. Results and discussion

4.1. Ignition delay time

Ignition delay times of farnesane-air-mixtures (synthetic air – 80 $\%_{vol}$ N_2, 20 $\%_{vol}$ O_2) were measured behind reflected shock waves at a dilution of 1:2 in nitrogen for two fuel equivalence ratios, φ = 1.0 and φ = 2.0. The measurements were carried out at pressures of around 16 bar and for temperatures between 800 and 1400 K. For deriving ignition delay time data experimentally, the time span between the initiation of the reactive system by the reflected shock front and the observed CH*-maximum emission at 431 nm served as an indicator, as described above (Fig. 2). In the simulations, the maximum of the calculated CH-concentration is chosen as the indicator for the ignition. For the simulations, in order to account for the pressure rise in the experiments, a pressure profile is used as input.

The comparison between the measured and predicted ignition delay times are presented in Fig. 9. The detailed reaction model captures well the trend of the measured ignition delay times in the entire temperature range. The predicted ignition delay times (curves) are in excellent agreement with the measured ones (symbols). Thus, the reaction model is capable of correctly reproducing the experimental obtained dependency of the ignition behavior on stoichiometry.

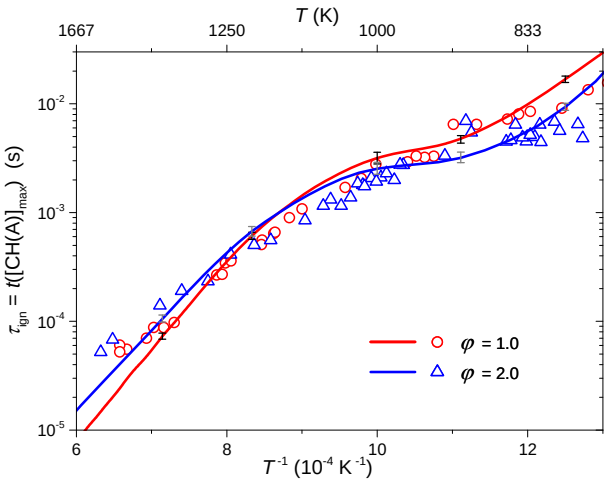

Fig. 9: Comparison of measured (symbols) and computed (curves) ignition delay times of farnesane-synthetic air mixtures *versus* reciprocal initial temperature T(t/s=0). The measurements are carried out at an initial pressure of p_i = p(t/s=0) = 16 bar and at two stoichiometries: φ = 1.0 (red circles) and φ = 2.0 (blue triangles). The error bars shown represent the uncertainty due to the post shock compression (see Fig. 2) by a deviation of ± 10 % in p(t/s>0) / p_i and were determined by calculating the ignition delay time using the new mechanism.

A global sensitivity analysis was performed for ignition delay times with three different initial temperatures selected depicting the low temperature, the intermediate as well as the high temperature regime covered within the present work. As an example, results are shown in Fig. 10 for stoichiometric farnesane-air-mixtures. For each temperature around ten important reactions showing maximum sensitivity are taken, usually that are reactions with normalized sensitivity coefficient larger than 0.3. At high temperatures, T = 1400 K, the reaction system is sensitive to the base hydrogen chemistry that generates radicals important for the radical pool build up, as known from previous studies. In addition, the ignition chemistry is sensitive to decomposition reactions of small branched

hydrocarbon formed from the farnesane decomposition channel. Among the reactions from the farnesane sub-mechanism, the farnesane decomposition channels leading to iC_9H_{19} + iC_6H_{13} and a-$iC_{10}H_{21}$ + iC_5H_{11} are important at this condition. At the intermediate temperature, T = 1000 K, the reaction sensitivity is similar to the one at high temperatures, in addition reactions involving HO_2 radicals are important. The ignition at low temperatures is shown to be sensitive to reactions of low temperature C_{15} alkyl peroxide formation and C_{15} alkyl peroxy radical decomposition reactions as well.

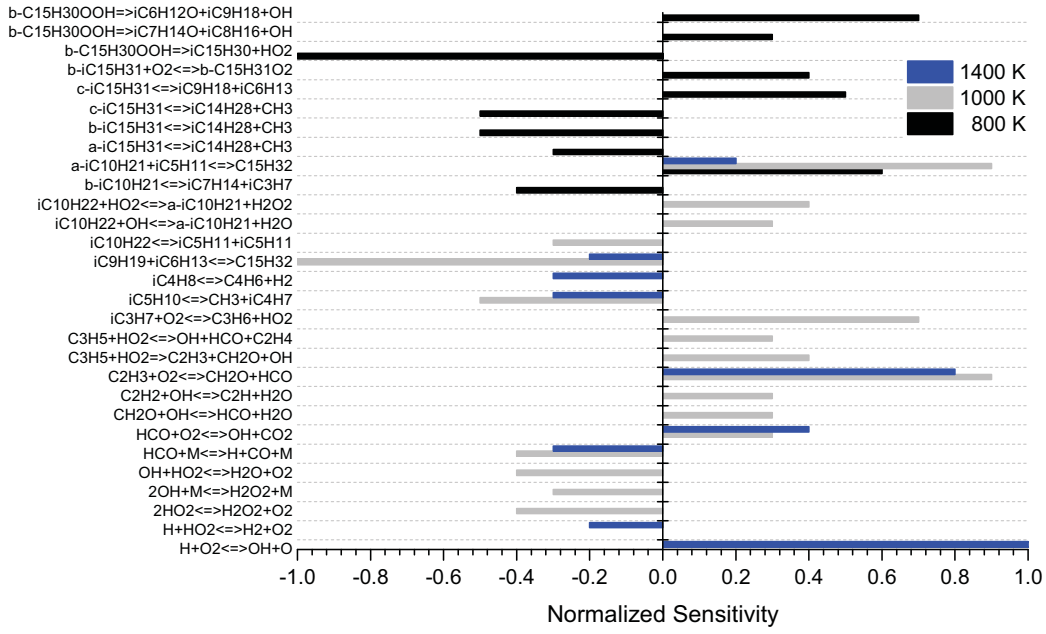

Fig. 10: Sensitivity analysis for ignition delay times presented in Fig. 9, at three different temperatures (T = 800, 1000 and 1400 K) for stoichiometric condition

4.2. Laminar flame speed

Laminar flame speeds of farnesane-air mixtures were calculated by using the farnesane mechanism discussed above. Figure 11 presents the comparison between measured burning velocities and calculated laminar flame speeds, at a preheat-temperature of T = 473 K at ambient (p = 1 bar) and elevated pressures (p = 3 and 6 bar) for fuel equivalence ratios φ ranging from φ = 0.6 to φ = 2.0. For

all pressure regimes studied, a good agreement between calculated and measured profile is seen with respect to the shape of the profile as well as to the position of the maximum value. The calculated flame speeds of farnesane within the lean to stoichiometric fuel range as well as up to φ values of approximately 1.5 are in excellent agreement with the measured values at p = 1 and p = 3 bar. For fuel richer mixtures (φ > 1.5), the measured burning velocities are underpredicted at both of these pressures by up to about 30 %. This shows that the reaction mechanism requires more attention at rich conditions.

At the highest pressure studied (p = 6 bar), the laminar flame speed simulations underpredict the measured burning velocities for all fuel-air mixtures. Although in this regime, the uncertainty range of the measurements is larger compared to the one at lower pressures, additional investigations are required on the above disagreement.

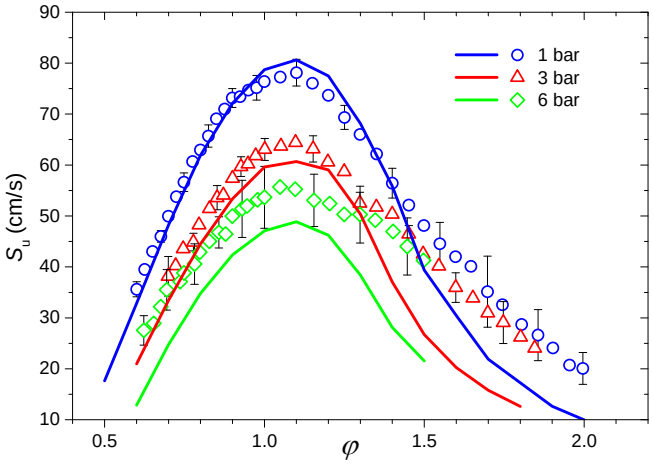

Fig. 11: Comparison of measured burning velocities (symbols) and simulated laminar flame speeds (curves) for farnesane-air mixtures at 473 K and p = 1 bar (blue), p = 3 bar (red), and p = 6 bar (green)

4.3. Important fuel destruction pathways

In order to get more insight into the consumption routes of farnesane, a reaction path analysis is performed. Results of farnesane oxidation at stoichiometric flame condition are presented in Fig. 12, for p = 1 bar. We follow the main decomposition paths starting from the heavier primary species to

smaller C_2- and C_3-hydrocarbon species and identify key species alongside. The integral rate shows that the decomposition reactions of farnesane are prominent at the given condition forming smaller $iC_{10}H_{21}$ as major product followed by iC_9H_{11}, iC_6H_{13} and iC_5H_{11} radicals. In a minor reaction channel, at given condition, the abstraction reaction by H-atoms is seen to produce secondary $C_{15}H_{31}$ radicals.

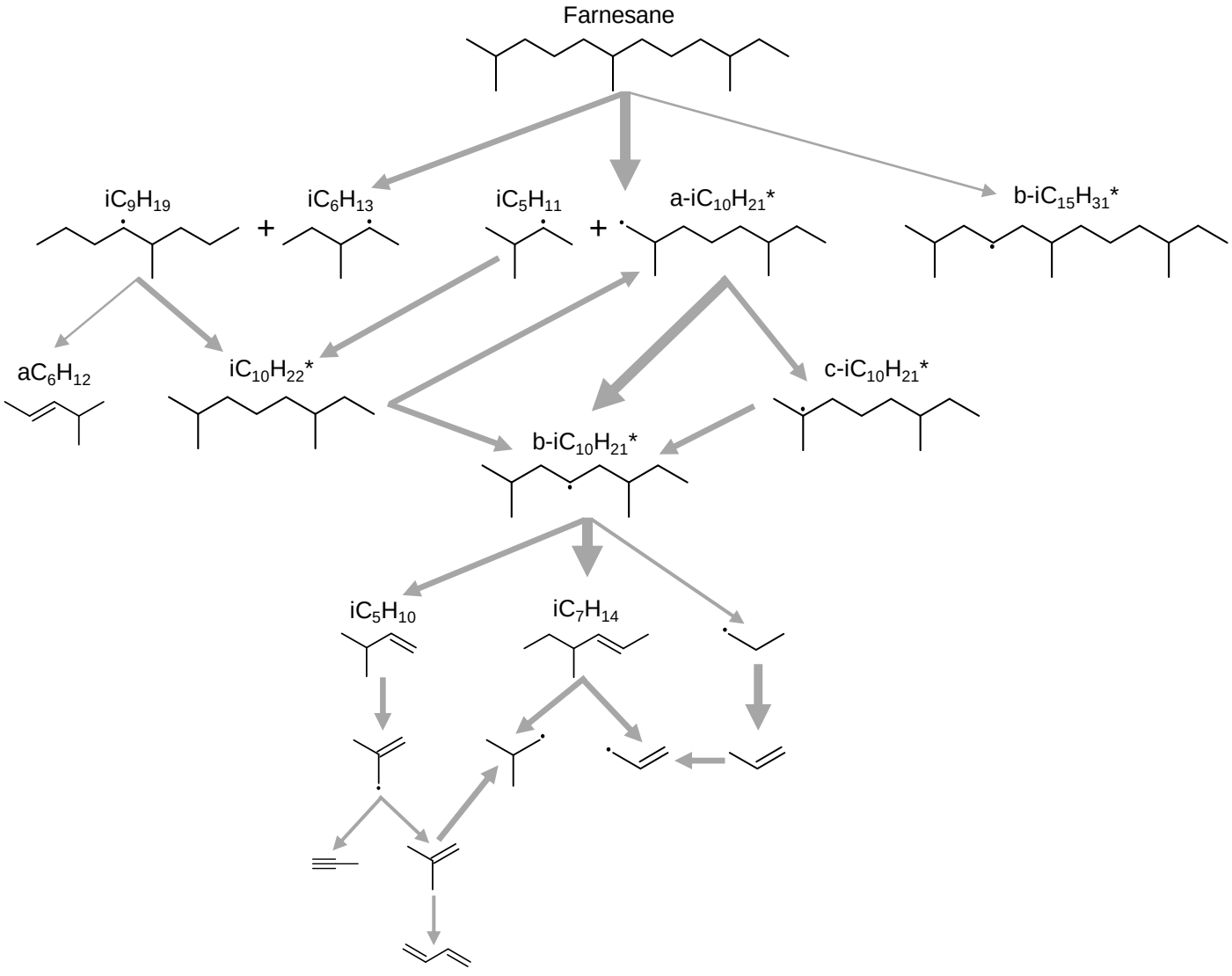

Fig. 12: Integral rate of production analysis showing fuel consumption for stoichiometric laminar flame condition, the thickness of arrows represents the importance of the reaction path, *refers to lumped species (structure of isomers available in supplementary material)

437 The main consumption of $iC_{10}H_{21}$ occurs by inter-isomerization reactions of this radical followed
438 by decomposition of the relatively stable secondary $iC_{10}H_{21}$ radical finally formed. The main decom-
439 position products form alkenes such as iC_5H_{10} and iC_7H_{14}, and iC_3H_7 radicals as well. The alkenes thus
440 formed undergo a β-scission leading to alkyl radicals and further smaller species, whereas iC_3H_7 yields
441 an alkene which further reacts to C_2-species. Thus, in summary, the typical pathways that occur are
442 consecutive H-abstraction followed by the scission of a C-H or C-C bond in β-position. The chemistry
443 of species smaller than C_2-C_3 is well known and not shown here.
444

445 ## 5. Summary and Outlook

446

447 The focus of the work is farnesane, a biofuel and blending component for Jet A-1 approved for the
448 use as a drop-in-fuel up to 10 % [8]. In this paper, a first reaction mechanism as well as new experi-
449 mental data for relevant global combustion properties for farnesane are presented. The considered
450 combustion properties are the ignition delay time and the laminar burning velocity, including a com-
451 parison to conventional Jet A-1. The measurements of the ignition delay times were performed for
452 two different stoichiometries (φ = 1.0 and φ = 2.0), each at a temperature range from about 800 to
453 1400 K and initial pressure of 16 bar. The laminar burning velocity were measured at a constant pre-
454 heat temperature of 473 K for three different pressures (1, 3 and 6 bar) in a stoichiometric range
455 from φ = 0.6 to φ = 2.0 for 1 bar and a slightly smaller range for elevated pressures. The comparison
456 to Jet A-1 for both the ignition delay times (Fig. 3) and the laminar burning velocity (Fig. 7) shows a
457 good agreement, concluding that farnesane has a combustion behavior similar to the one of the con-
458 ventional fuel Jet A-1. Only for temperatures below 1000 K farnesane shows slightly shorter ignition
459 delay times than Jet A-1.
460 The reaction mechanism was developed on the basis of an existing in-house mechanism for n- and
461 iso-alkanes up to C_{12} [32, 33], focusing on the prediction of the global combustion properties ignition
462 delay time and laminar flame speed (see Fig. 9 and Fig. 11 for results). The reproduction of the igni-

tion delay time by the reaction model match perfectly with the experiments also, the calculations of the laminar flame speeds at 1 and 3 bar with a φ-range from 0.6 to 1.5 are in a good agreement with the experimental results.

An improvement of the reaction model is required for the calculation of laminar flames at a pressure of 6 bar as well as for rich conditions. The recently published speciation data from Oßwald *et al.* [21] will be helpful for a further development of the mechanism, looking deeper into single reaction pathways.

6. Acknowledgement

The authors thank S. Scheuermann and J. Ortner from the Bundeswehr Research Institute for Materials, Fuels and Lubricants (WIWeB) in Erding (Germany) for suppling us with farnesane and also A. Zschocke from Deutsche Lufthansa AG. Furthermore we thank M. B. Raida for her help by measuring the laminar burning velocity as well as N. Ackermann, Ph. Coens and H. Dreyer for their experimental support in measuring the ignition delay times. A part of the measurements on Jet A-1 was performed within the project ALFA-BIRD: EUFP7/2007-2013, grant agreement no° 213266.

7. References

[1] Blakey S, Rye L, Wilson CW. Aviation gas turbine alternative fuels: A review. Proc Comb Inst 2011;33(2):2863-85.

[2] Braun-Unkhoff M, Riedel U. Alternative fuels in aviation. CEAS Aeronaut J 2015;6:83-93.

[3] Braun-Unkhoff M, Riedel U, Wahl C. About the emissions of alternative jet fuels. CEAS Aeronaut J 2017; in Press: doi:10.1007/s13272-016-0230-3.

[4] Kick T, Kathrotia T, Braun-Unkhoff M, Riedel U. An experimental an modeling study of laminar flame speeds of alternative aviation fuels. Proc ASME Turbo Expo 2011;GT2011-45606.

[5] Kick T, Herbst J, Marquetand J, Braun-Unkhoff M, Naumann C, Riedel U. An experimental and modeling study of burning velocities of possible future synthetic jet fuel. Energy 2012;43(1):111-23.

[6] Dagaut P, Karsenty F, Dayma G, Diévart P, Hadj-Ali K, Mzé-Ahmed A et al. Experimental and detailed kinetic model for the oxidation of a Gas to Liquid (GtL) jet fuel. Comb Flame 2014;161(3):835-47.

[7] Braun-Unkhoff M, Dembowski J, Herzler J, Karle J, Naumann C, Riedel U. Alternative fuels based on biomass: An experimental and modeling study of ethanol co-firing to natural gas. Proc ASME Turbo Expo 2014: Turbine Technical Conference and Exposition;GT2014-26714.

[8] Zschocke A, Scheuermann S, Ortner J. High Biofuel Blends in Aviation (HBBA), http://www.hbba.eu; 2015 [accessed 07.11.16].

[9] ATAG. Beginner's Guide to Aviation Biofuels, http://www.atag.org/our-publications/latest.html; 2011 [accessed 07.11.16].

[10] aireg. Milestone for sustainable aviation: innovative fuel gains approval, http://www.aireg.de/en/press-releases/333-milestone-for-sustainable-aviation-innovative-fuel-gains-approval.html; 2014 [accessed 07.11.16].

[11] Amyris. trans-beta-Farnesene, https://farnesene.net; [accessed 14.12.15].

[12] Sapp M. First-ever commercial flight on farnesene flies Orlando to Sao Paolo, http://www.biofuelsdigest.com/bdigest/2014/07/31/first-ever-commercial-flight-on-farnesene-flies-orlando-to-sao-paolo/; 2014 [accessed 21.10.16].

509 [13] Yee A. Airlines Fly the Skies on a Sugar High,
510 http://www.nytimes.com/2014/10/08/business/energy-environment/airlines-fly-the-skies-on-a-
511 sugar-high.html?_r=0; 2014 [accessed 21.10. 16].

512 [14] Lufthansa Group. Sustainable alternative fuels,
513 https://www.lufthansagroup.com/en/responsibility/climate-and-environmental-
514 responsibility/keroseneandemissions/biofuel-at-lufthansa.html; [accessed 07.11.16].

515 [15] Lane J. Cathay sets biofuels-based flight record, as new A350 ushers in renewable jet era at
516 Hong Kong, http://www.biofuelsdigest.com/bdigest/2016/05/31/cathay-sets-biofuels-based-
517 flight-record-as-new-a350-ushers-in-renewable-jet-era-at-hong-kong/; 2016 [accessed
518 21.10.16].

519 [16] Conconi CC, Crnkovic PM. Thermal behavior of renewable diesel from sugar cane, biodiesel,
520 fossil diesel and their blends. Fuel Process Technol 2013;114:6-11.

521 [17] Won SH, Dooley S, Veloo PS, Wang H, Oehlschlaeger MA, Dryer FL et al. The combustion proper-
522 ties of 2,6,10-trimethyl dodecane and a chemical functional group analysis. Comb Flame
523 2014;161(3):826-34.

524 [18] Tekawade A, Oehlschlaeger MA. An experimental study of the spray ignition of alkanes. Fuel
525 2016;185:381-93.

526 [19] Valco DJ, Min K, Oldani A, Edwards T, Lee T. Low temperature autoignition of conventional jet
527 fuels and surrogate jet fuels with targeted properties in a rapid compression machine. Proc
528 Comb Inst 2016; in Press: http://dx.doi.org/10.1016/j.proci.2016.05.032.

529 [20] Millo F, Bensaid S, Fino D, Castillo Marcano SJ, Vlachos T, Debnath BK. Influence on the perfor-
530 mance and emissions of an automotive Euro 5 diesel engine fueled with F30 from Farnesane.
531 Fuel 2014;138:134-42.

[21] Oßwald P, Whitside R, Schäffer J, Köhler M. An experimental flow reactor study of the combustion kinetics of terpenoid jet fuel compounds: Farnesane, p-menthane and p-cymene. Fuel 2017;187:43-50.

[22] ALFA-BIRD. Alternative fuels and biofuels for aircraft. EUFP7/2007-2013, grant agrrement no° 213266. http://www.alfa-bird.eu-vri.eu/; [accessed 27.01.17]

[23] Herzler J, Jerig L, Roth P. Shock tube study of the ignition of lean n-heptane/air mixtures at intermediate temperatures and high pressures. Proc Comb Inst 2005;30(1):1147-53.

[24] Green WH, Allen JW, Beat A, Buesser R, Ashcraft W, Beran GJ et al. RMG-Reaction Mechanism Generator, http://rmg.mit.edu/molecule_search; 2015 [accessed 07.11.16].

[25] Goos E, Burcat A, Ruscic B. Ideal Gas Thermochemical Database with updates from Active Thermochemical Tables, ftp://ftp.technion.ac.il/pub/supported/aetdd/thermodynamics, mirrored at http://garfield.chem.elte.hu/Burcat/burcat.html; [accessed 28.03.12].

[26] Ciezki HK, Adomeit G. Shock-Tube Investigations of Self-Ignition of n-Heptane-Air Mixtures Under Engine Relevant Conditions. Comb Flame 1993;93(4):412-33.

[27] Andrews GE, Bradley D. Determination of Burning Velocities: A Critical Review. Comb Flame 1972;18(1):133-53.

[28] Eberius H, Kick T. Stabilization of Premixed, Conical Methane Flames at High Pressure. Ber Bunsenges Phys Chem 1992;96(10):1416-19.

[29] Aschenbrenner H, Nieken U. Institut für Chemische Verfahrenstechnik (ICVT), University Stuttgart, Germany.

[30] Hui X, Kumar K, Sung C-J, Edwards T, Gardner D. Experimental studies on the combustion characteristics of alternative jet fuels. Fuel 2012;98:176-82.

554 [31] Won SH, Veloo PS, Dooley S, Santner J, Haas FM, Ju Y et al. Predicting the global combustion
555 behaviors of petroleum-derived and alternative jet fuels by simple fuel property measurements.
556 Fuel 2016;168:34-46.

557 [32] Slavinskaya N, Riedel U, Saibov E, Herzler J, Naumann C. Kinetic Surrogate Model for GTL Kero-
558 sene. Proc 52nd AIAA Aerospace Sciences Meeting and Exhibit 2014;AIAA2014-0126.

559 [33] Knyazkov DA, Slavinskaya N, Dmitriev AM, Shmakov AG, Korobeinichev OP, Riedel U. Structure
560 of an n-heptane/toluene flame: Molecular beam mass spectrometry and computer simulation
561 investigations. Combust Explos Shock Waves 2016;52(2):142-54.

562 [34] Curran HJ, Gaffuri P, Pitz WJ, Westbrook CK. A Comprehensive Modeling Study of Iso-Octane
563 Oxidation. Comb Flame 2002;129(3):253-80.

564 [35] Ratkiewicz A, Truong TN. Kinetics of the C–C Bond Beta Scission Reactions in Alkyl Radical Reac-
565 tion Class. J Phys Chem A 2012;116(25):6643-54.

566 [36] Awan IA, McGivern WS, Tsang W, Manion JA. Decomposition and Isomerization of 5-Methylhex-
567 1-yl Radical. J Phys Chem A 2010;114(30):7832-46.

568 [37] Kintech Laboratory. Chemical Workbench®, http://www.kintechlab.com/products/chemical-
569 workbench/; 2013 [accessed 07.11.16].